Journal of Environmental Management 295 (2021) 113319

Contents lists available at ScienceDirect

Journal of Environmental Management

journal homepage: www.elsevier.com/locate/jenvman

Scots pine stands biomass assessment using 3D data from unmanned aerial vehicle imagery in the Chernobyl Exclusion Zone

Dmytrii Holiaka [a], Hiroaki Kato [b], Vasyl Yoschenko [c,*], Yuichi Onda [b], Yasunori Igarashi [c], Kenji Nanba [c], Petro Diachuk [a], Maryna Holiaka [a], Roman Zadorozhniuk [a], Valery Kashparov [a], Ihor Chyzhevskyi [d]

[a] Ukrainian Institute of Agricultural Radiology, National University of Life and Environmental Sciences of Ukraine, Mashinobudivnykiv Str. 7, Chabany, Kyiv Region, 08162, Ukraine
[b] Center for Research in Isotopes and Environmental Dynamics at University of Tsukuba, 1 Tennodai, Tsukuba, 305-8577, Japan
[c] Institute of Environmental Radioactivity at Fukushima University, 1 Kanayagawa, Fukushima, 960-1296, Japan
[d] State Specialized Enterprise Ecocentre, State Agency of Ukraine on Exclusion Zone Management, Shkil'na Str. 4, Chernobyl, Kyiv Region, 07270, Ukraine

ARTICLE INFO

Keywords:
Forest stand parameters
Canopy height model (CHM)
Remote biomass sensing
Airborne survey
Unmanned aerial vehicle (UAV)
GIS

ABSTRACT

Thirty-five years after the accident, large forest areas in the Chernobyl Exclusion Zone still contain huge amounts of radionuclides released from the Chernobyl Nuclear Power Plant Unit 4 in April 1986. An assessment of the radiological and radioecological consequences of persistent radioactive contamination and development of remediation strategies for Chernobyl forests imply acquiring comprehensive data on their contamination levels and dynamics of biomass inventories. The most accurate forest inventory data can be obtained in ground timber cruises. However, such cruises in radioactive contaminated forest ecosystems in the Chernobyl Exclusion Zone result in radiation exposures of the personnel involved, which means the need for development of the remote sensing methods. The purpose of this study is to analyze the applicability and limitations of the photogrammetric method for the remote large-scale monitoring of aboveground biomass inventories. Based on field measurements, we estimated the biomass inventories in 31 Scots pine stands including both artificial plantations and natural populations. The stands differed significantly in age (from a few years in natural populations to 115 years in the oldest plantation), productivity (from 0.4 to 19.8 kg m^{-2}), mean height (from 4.1 to 36 m), and other parameters. Photogrammetric data were obtained from the same stands using unmanned aerial vehicle (UAV). These data were then processed using two approaches to derive the canopy height model (CHM) parameters which were tested for correlation with the aboveground biomass inventories. In the first approach, we found that the inventories correlated well with the mean value of CHM of the site ($R^2 = 0.79$). In the second approach, the total aboveground biomass was approximated by a function of the average height of trees detected at the site and the total crown projection area ($R^2 = 0.78$). Among other local parameters, the total crown projection area was identified as the major factor impacting the accuracy of the aboveground biomass inventory estimates from the UAV survey data in both approaches. In the dense stands with the high total crown projections areas (more than 0.90), the average relative deviations of the UAV-based aboveground biomass estimates from the results of the field measurements were close to 0, which means the adequate accuracy of the UAV surveys data for radioecological monitoring purposes. The relative deviations of the UAV-based estimates in both approaches increased in the stands consisting of separated groups of trees, which indicates potential limitation of the approaches and need for their further development.

1. Introduction

The recent rapid development of low-cost unmanned aerial vehicle (UAV) technologies and significant improvements in digital imaging and processing, along with increases in computing capacities and geo-positioning accuracy, have greatly expanded capabilities of high-resolution remote sensing of the surface. In particular, in the last decade, considerable efforts have been directed toward the elaboration

* Corresponding author.
E-mail address: r705@ipc.fukushima-u.ac.jp (V. Yoschenko).

https://doi.org/10.1016/j.jenvman.2021.113319
Received 22 March 2021; Received in revised form 9 July 2021; Accepted 16 July 2021
Available online 22 July 2021

of automated forest inventory methods using UAVs. An overview of current remote sensing methods in forestry (satellite, aircraft, and UAV) and a comparison of their effectiveness can be found in a recent comprehensive review by Surový and Kuželka (2019). The UAV-based methods typically use airborne optical cameras or airborne LIDAR (Light Detection and Ranging) scanning systems to acquire the 3D datasets enabling detection of the individual trees (Li et al., 2012; Mohan et al., 2017; Eysn et al., 2015; Keefe et al., 2019) and deriving certain tree and stand parameters (White et al., 2013; Wallace et al., 2016; Goodbody et al., 2017a, b; Miller et al., 2017; Panagiotidis et al., 2017; Puliti et al., 2017; Abdollahnejad et al., 2018; Brovkina et al., 2018; Giannetti et al., 2018; Lin et al., 2018; Otero et al., 2018; Surový and Kuželka, 2019; Piermattei et al., 2019; Wang et al., 2019; Huylenbroeck et al., 2020; Kuželka et al., 2020; Ramalho de Oliveira et al., 2021, and many others). The use of LIDAR makes measurement costs more expensive, while the use of photogrammetric data, especially data from digital single-lens reflex cameras, provides nearly as much accuracy in detecting individual trees (Ramalho de Oliveira et al., 2021). A recent comparison (Wallace et al., 2016) has shown that both airborne laser scanning and photogrammetric data acquisition can be successfully used for forestry measurements, although each has certain advantages, and the choice between the methods may depend on the survey budget and objectives. Being much less expensive, the photogrammetric method is usually recommended for small-to-medium scale and short-term forest structure measurements. Compared to ground timber cruises, UAV surveys require less time and less labor; moreover, such surveys can be carried out in forest areas where access is difficult, or working conditions are dangerous. In this paper we will discuss the application of the UAV photogrammetric method.

Photogrammetric datasets can be visualized using various software tools enabling creation of digital elevation models and digital surface models (DEM and DSM, respectively), as well as orthophotomaps based on processing of a large number of digital photos taken aerial over the surveyed area and their metadata. Available tools and algorithms allow to build canopy height models (CHM) for identification of tree tops (Mohan et al., 2017), measurement of their heights (Wallace et al., 2016), projection and measurement of crown areas (Panagiotidis et al., 2017), distinguishing tree species based on crown shape (Cruzan et al., 2016; Brovkina et al., 2018), and deriving other numerical and qualitative information about the surveyed forest stand (Puliti et al., 2017; Giannetti et al., 2018; Otero et al., 2018; Abdollahnejad et al., 2018; Surový and Kuželka, 2019; Piermattei et al., 2019). However, the accuracy of UAV measurements is satisfactory high in areas where trees and shrubs grow sparsely, such as parks and old forest stands, but it is rather low when surveying in areas with dense deciduous forests (Goodbody et al., 2017a, b). In general, the overall performance of the method depends on the equipment used (Ramalho de Oliveira et al., 2021) and can be affected by factors specific to the stand being surveyed, such as the complexity of the vertical structure of the stand, diversity of plant species, etc., as well as ambient conditions such as windy weather, fog, shade, and temperature variations (Mohan et al., 2017).

As already noted, in certain circumstances, the application of UAV-based methods has advantages in performing field measurements. For example, UAV surveys can be suggested for acquiring radioecological monitoring data and planning forestry management activities in the Chernobyl Exclusion Zone (ChEZ), a vast area in Ukraine, Belarus, and Russia, that remains heavily contaminated with long-lived radionuclides released from the Chernobyl Nuclear Power Plant as a result of the accident on April 26, 1986 (Kashparov et al., 2003, 2018; 2020; UNSCEAR, 2008). Forests cover about 60% of the ChEZ territory and play a role of an environmental repository of radioactive fallout (Nikonchuk, 2015; Yoschenko et al., 2019, 2020). Currently, biota in Chernobyl forests accumulates large amounts of radionuclides (Shcheglov et al., 2014). Aboveground biomass can contain up to 30–50% of total ecosystem inventories of ^{90}Sr; in pine forests, significant fractions of total ^{137}Cs inventories are localized litter (Holiaka et al., 2020b; Yoschenko et al., 2019, 2020). The inventories may further increase due to biomass growth (Goor et al., 2007).

Being excluded from the commercial utilization, Chernobyl forests are also inadequately maintained, resulting in the accumulation of large amounts of dry dead biomass and therefore creating favorable conditions for the development of large-scale wildfires which periodically occur in the exclusion zone (Ager et al., 2019) and show an increasing trend in their severity. Moreover, natural forests succession and broken forest roads have made it difficult for fire crews to access many areas. As a result, a wildfire in April 2020 destroyed or damaged terrestrial ecosystems over a huge area of about 67,000 ha (SAUEZM, 2021). Such fires rise concerns about the potential remobilization of radionuclides from burning forest biomass into the smoke plume and their further spread to adjacent lands (Kashparov et al., 2000, 2017, 2017; Yoschenko et al., 2006) and even to remote areas (Evangeliou et al., 2014, 2016; Talerko et al., 2021), and about the wash-off of fire products such as ash into surface waters (Igarashi et al., 2020). In the most contaminated areas, many forests are artificial overstocked stands that have significantly higher biomass inventories than typical forests in the region. In the absence of economic activity, forests in the exclusion zone spread to abandoned agricultural lands, forming new forest stands. The above-mentioned processes cause redistribution of radionuclides in the environment of the ChEZ. Assessment of relevant radiological and radioecological consequences requires data on biomass inventories and dynamics in compartments of forest ecosystems, especially in fast growing young stands. On the other hand, measures must be taken to minimize the radiation exposure of the personnel involved, which can be achieved through the widespread use of UAV surveys of contaminated forests.

The dominant tree species, spreading on about 60% of the forested area in Chernobyl, is Scots pine (Nikonchuk, 2015; Yoschenko et al., 2019, 2020). Pine stands are presented by artificial plantations of different ages and by natural populations that colonized abandoned agricultural land after the Chernobyl accident. Accordingly, stand parameters such as plantation density, age, and vertical structure vary greatly within the ChEZ. In addition, this species is known for its high radiosensitivity: chronic radiation causes severe morphological transformations in young trees. The typical morphological abnormality is cancellation of the apical dominance, which appears as replacement of a single tree trunk by several equipollent branches. The frequency of abnormal transformation is high throughout the ChEZ reaching almost 100% in the most contaminated places (Yoschenko et al., 2011). This transformation suppresses the tree growth and affects stand productivity. On the other hand, it can also affect the accuracy of biomass estimates derived from the UAV survey data due to the increased difficulty in detecting actual tree tops and the difference in parameters between normal and abnormal trees in the surveyed stands.

As can be seen from the literature reviewed above, remote sensing methods should be chosen and may need to be adjusted according to the specific conditions of the area under study. The aim of the present paper is to test the applicability and identify the factors impacting the accuracy of UAV-based photogrammetric approaches for estimation of aboveground biomass inventories in the Chernobyl pine forest stands of various origin with different proportions of abnormal trees. The obtained results can be used for large-scale forest surveys within the framework of a comprehensive collaborative study aimed at evaluation of the current radioecological situation in the Chernobyl Exclusion Zone (http://www.ier.fukushima-u.ac.jp/satreps/index.html).

2. Materials and methods

2.1. Experimental sites

The study was carried out in the forest areas managed by the State Specialized Enterprise “Pivnichna Puscha” and by the Chernobyl Radiation and Ecological Biosphere Reserve at the distances 5–12 km from

the Chernobyl Nuclear Power Plant industrial site (Supplementary materials, Fig. S1). Between August 2017 and September 2019, we conducted UAV photogrammetric surveys and ground-based measurements at 31 experimental sites located in 13 pine stands. Radionuclide soil depositions in the studied ecosystems varied from 170 to 17,300 kBq m^{-2} for ^{137}Cs (in the 30 cm soil layer) and from 50 to 7520 kBq m^{-2} for ^{90}Sr (in the 1 m deep soil layer) (Kashparov et al., 2018, 2020; Holiaka et al., 2020a).

The experimental sites were selected within homogeneous stands of pine of different ages. We established these sites as circular sampling plots as recommended for forest inventory purposes (Kangas and Maltamo, 2006). The plot areas S_{site} (250 m^2, 500 m^2, 1000 m^2 or 5000 m^2) were chosen based on the plantation densities at the sites to provide at least 20 trees in young and sparsely populated natural stands, and more than 30 trees in closed high productive forest stands. According to silvicultural recommendations (e. g., Anuchin, 1982; Kashpor and Strochinskii, 2013), sample plots of this size can provide sufficient accuracy in estimating stand parameters in the ground timber cruises. At most of our experimental plots, the actual number of trees was more than twice as high as the above figures. Thus, in this study we compare the results of the UAV-based measurements with those obtained by the conventional forest inventory method.

Geographic coordinates of the sampling areas were determined using a Dakota 10 GPS navigator (Garmin Ltd., USA). Forest stand parameters were calculated from measurements of diameters at 1.3 m heights (diameter at the breast height) of all trees in the sampling area, and from height measurements of 12–30 model trees in dense stands aged over 30 years, or all trees in other stands. The locations of individual trees within the sampling areas and their heights were measured manually using a TruPulse 360B laser-optical rangefinder and MapSmart software (Laser Technology, Inc., USA).

Stand parameters were calculated using appropriate forest mensuration approaches (Anuchin, 1982). Relative stocking, RS, and inventories of trunk wood with bark were estimated according to the recommendations on forest taxation adopted in Ukraine (Kashpor and Strochinskii, 2013). Relative stocking is defined as a ratio of the stand basal area to the reference value of the basal area that corresponds to the 95 percentile of the stands of the given species, height and quality in the region.

Within each sampling plot, all trees were examined for severe morphological abnormalities (cancellation of the apical dominance and strong deformations of the tree trunk).

The results of ground-based observations at the experimental sites along with the calculated forest mensuration parameters are presented in Supplementary materials (Table S1).

2.2. Airborne surveys

Airborne surveys at the experimental sites were carried out using a *Phantom 4 Pro* drone (SZ DJI Technology Co., Ltd.) in standard specification, equipped with 1″ CMOS camera (20M effective pixels, lenses angled to 84°). To determine the optimum survey altitude, we conducted test surveys at several locations at 30 m, 40 m, 80 m, 120 m, 250 m and 500 m. The test results showed that the minimum flight altitude at which aerial photos taken over homogeneous forested areas could be reliably aligned was 120 m, and all further surveys were conducted at this altitude.

The flight routes were built and uploaded into the drone's memory using the Android mobile app Litchi (https://flylitchi.com/hub). Based on the results of the test surveys, in order to guarantee at least 50% overlap of neighboring images, the surveys were performed in the following mode: distance 40–45 m between UAV tracks, interval 2 s between the photo shots, maximum flight speed 16.6 km h^{-1}. The image size was set to 5472 × 3648 pixels.

The accuracy of measurement of geographic coordinates in forests using GPS navigators is affected by interference of the satellite signal with tree canopies (Keefe et al., 2019). For this reason, we placed special targets in the open spaces at the sites, and further specified the coordinates of the centers of the sites using the coordinates of these targets derived from the orthophotomaps.

2.3. Data processing

Two basic approaches can be used to estimate biomass inventories in forest ecosystem compartments using UAV photogrammetric data. In the first approach, the canopy height model (CHM) of a forest area is analyzed to identify individual trees and shrubs and estimate their parameters, and then use these parameters to calculate compartment biomasses within the area using empirical tree growth relationships (Lin et al., 2018). In the present paper, we develop this approach over our earlier study (Holiaka et al., 2018). In the second approach, CHM distribution parameters in the studied area are determined to directly estimate forest indices, including biomass inventory (Puliti et al., 2018). The latter may be the only efficient approach for remote assessment of biomass inventories in dense stands, where accurate segmentation of CHM into individual plants is hardly possible.

The scheme of data processing in this study is presented in Fig. 1. We used the results of ground-based measurements as "true" estimates of the biomass inventories in the aboveground compartments of the stands under study. The results of the UAV surveys were processed in the two approaches mentioned above. In the CHM approach, we attempted to establish direct correlations between the biomass estimates and certain statistical parameters (arithmetic mean AM, standard deviation STD, standard error, coefficient of variations CV, asymmetry, excess, sum, minimum and maximum, range, etc.) of the CHM of the studied stands without segmenting them for individual tree canopies. The applicability of the derived from the photogrammetric data CHM indices, such as mean and median CHM, maximum of CHM and others, for estimating aboveground biomass inventories (mainly in tropical forests) has been shown in many studies, e.g., Ota et al. (2015), Zahawi et al. (2015), Kachamba et al. (2016), Miller et al. (2017), Jayathunga et al. (2019), and others. However, it is clear that the parameters of the correlation relationships and the accuracy of the method can vary between species, stands of different ages, etc. Here, we tested the approach for specific conditions in the ChEZ. Local conditions also affect the rate of detection of individual trees and the accuracy of determination of their heights from UAV survey data (Surový and Kuželka, 2019). In the ITD (individual tree detection) approach, we quantified heights of the individual trees that could be detected in the CHM and the total crown projection areas, and searched for correlations between these parameters and the biomass estimates. Details of the biomass assessment and processing of aerial images are presented below.

2.3.1. Estimation of aboveground stand biomass using ground-based measurements

The biomass inventories in the compartments of the studied pine stands (d.w.) were calculated using empirical regression dependencies (Eqs. (1)–(7)) established for typical artificial Scots pine plantations of the study region (Lakida, 2013):

$$M_{trunk} = 0.1441 \cdot DBH^{-0.191} \cdot H^{1.748} \cdot RS^{1.008} \quad (1)$$

where M_{trunk} is the barked wood biomass, kg m^{-2},

$$M_{needle} = 0.5096 \cdot DBH^{0.596}\, H^{-0.526} \cdot RS^{0.792} \quad (2)$$

where M_{needle} is the needle biomass, kg m^{-2},

$$M_{branch} = 0.1709 \cdot DBH^{1.111}\, H^{-0.506} \cdot RS^{0.332} \quad (3)$$

where M_{branch} is the branch biomass, kg m^{-2}.

and for the natural stands of Scots pine:

$$M_{trunk} = 0.2288 \cdot DBH^{-0.162} \cdot H^{1.592} \cdot RS^{1.018} \quad (4)$$

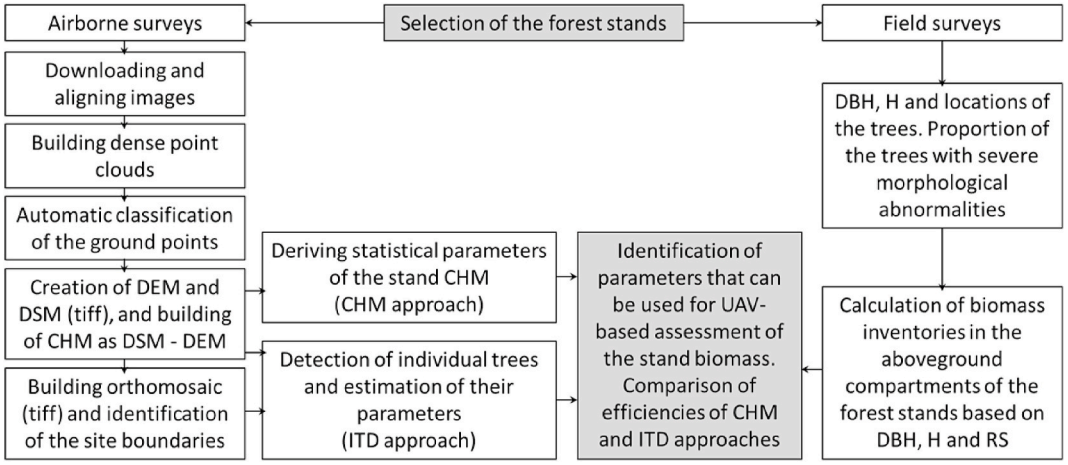

Fig. 1. Data acquisition and processing workflow.

$$M_{needle} = 0.2625 \cdot DBH^{-0.0013} \cdot H^{0.138} \cdot RS^{0.722} \quad (5)$$

$$M_{branch} = 0.3056 \cdot DBH^{0.675}\, H^{-0.355} \cdot RS^{0.434} \quad (6)$$

The total aboveground biomass M_{AG} is the sum of the biomass inventories in the three compartments:

$$M_{AG} = M_{trunk+}M_{needle+}M_{branch} \quad (7)$$

2.3.2. Processing of UAV survey data

Stereo photogrammetric processing of aerial images of the studied stands and creation of 3D models (DSM and DEM raster images) and orthophotomaps were performed using *Agisoft Photoscan 1.4.5* software. DEM were constructed after automatic classification of the dense point clouds. Raster CHM images were obtained by subtracting DEM from the corresponding DSM using the raster image calculator in *QGIS 3.4.11* software (Supplementary materials, Fig. S2-S5), and their distribution parameters were tested for correlations with the biomass inventories in the CHM approach.

Similarly to other studies (e.g., Panagiotidis et al., 2017; Mohan et al., 2017), detection of individual trees at CHM was performed using algorithms enabling identification of local maxima and individual tree canopy delineation. To implement the ITD approach, the raster CHM images were processed using ForestTools package from the Comprehensive R Archive Network (CRAN) repository to identify trees (local maxima at CHM) and measure their heights, and to segment the CHM into the crown projections. The corresponding R-script is presented in Appendix S1. The sum of the crown projections was used to estimate their overlap (Plowright, 2020; Plowright and Roussel, 2020). To separate neighboring trees, we used filtering radii for finding local maxima, r_F, as well as applied a minimum height index (*tree_h*) at which a local maximum could be interpreted as a tree top. The filtering radius is a key parameter that depends on the CHM value of a given local maximum (Holiaka et al., 2018) and determines the minimum distance to a neighboring maximum at which both neighboring maxima are recognized as separate trees. Its application is aimed at minimizing commission errors (false interpretation of local maxima, e.g. branch tops, as individual trees).

In artificial plantations, pine seedlings are planted in nodes in a regular grid, usually 0.7 m × 1.0 m, and therefore the filtering radius in young plantations can simply be set at 0.7 m. Over time, however, some of the trees are eliminated from the plantations through the natural processes and thinning, which increases the average distance between the trees. Like natural populations, trees in mature plantations can form dense groups separated by open or less populated spaces, making it impossible to apply a single filtering radius that would eliminate commission errors without introducing omission errors (failure to detect all trees).

In the simplified case of a uniform distribution of n pine trees of the same size within the area S_{site} (i.e. the trees are each localized in the centers of the equal square cells without empty spaces between such cells) the distance between the neighboring trees is equal to

$$r_n = \sqrt{\frac{S_{site}}{n}}, \quad (8)$$

and assigning this value to r_F must enable detection of all trees. In our approach, we tested the use of r_n as characteristic values to obtain the filtering radius for detecting individual trees in real forest stands where the spatial distribution patterns of trees are not known a priori. For each study site, we calculated the value of r_n (eq. (8)) using the results of ground-based measurements. Applied as r_F for a given stand, it would enable detection of trees growing outside of dense groups. False detections would still be possible from shrubs and fallen trees in open areas, and from branches ranging outside r_F from large trees growing separately in open places. We then assumed that the average distance between trees might depend on their heights, and analyzed the dependence of r_n on the average tree heights H measured in the stands. Finally, based on the lowest r_n values obtained at different H, as shown in section 3.3, $r_F(H)$ dependencies were derived for the artificial and natural stands and used to set the filtering radii as function of the CHM pixel height. Note that in this formulation, the ITD approach does not imply that all the trees in the stand need or can be detected. To address effect of omission errors, in addition to the average height of detected trees in the stand, we introduced the total tree crown projection area p_{crown} into the regression equations for the biomass inventory estimates:

$$p_{crown} = \sum A_{crown}/S_{site} \quad (9)$$

where A_{crown} denotes the crown projection areas of individual trees.

2.3.3. Analysis of the statistical validity of the obtained models

The statistical validity of the obtained regression models for the aboveground biomass estimation from the UAV survey data was analyzed using the F-test (F-value) and the coefficient of determination R^2. The parameters of the equations were analyzed for significance using *t*-test. As in other studies (e.g., Navarro et al., 2020), the similarity of the obtained distributions of the model results and the results of the ground-based measurements was assessed using Wilcoxon signed rank test, since the Shapiro-Wilk test (Shapiro and Wilk, 1965) demonstrated absence of normal distributions for inventories of branches and needles

at p = 0.05. Root Mean Square Error (*RMSE*) and *Bias* were used to quantify the deviation of UAV-based biomass estimates $\hat{y}_i$ from the biomass inventories calculated from the ground measurements y_i (Su et al., 2020):

$$RMSE = \sqrt{\frac{\sum_{i=1}^{n_{pair}} (\hat{y}_i - y_i)^2}{n_{pair}}} \quad (10)$$

$$RMSE(\%) = \frac{RMSE}{\bar{y}} \times 100 \quad (11)$$

$$Bias = \frac{\sum_{i=1}^{n_{pair}} (\hat{y}_i - y_i)}{n_{pair}} \quad (12)$$

$$Bias(\%) = \frac{Bias}{\bar{y}} \times 100 \quad (13)$$

where n_{pair} is the number of observations, and $\bar{y}$ is the arithmetic mean of all y_i.

Statistical analyses of all results were performed in *Microsoft Excel 365* and *RStudio 1.3* using the *R 4.0* programming language (version 4.0.5 https://www.r-project.org/).

3. Results

3.1. Estimates of biomass inventories using ground-based measurement results

The aboveground biomass inventories at the experimental sites, calculated using data from Table S1 (Supplementary materials) and equations (1)–(7), are presented in Table 1. The total biomass inventory values are uniformly distributed over a wide range from about 1 kg m^{-2} in several natural populations with low relative stocking values and a high proportions of abnormal trees to nearly 20 kg m^{-2} in mature artificial forest stands at the sites ChZ-4 and ChZ-14. The greatest variations in total biomass inventories and compartment inventories were observed in the young open stands where confidence intervals at p-value of 0.05 reached 50% of the predicted inventory values, while in the closed artificial stands confidence intervals at p = 0.05 were 18–22% of the predicted values. In all stands, with the exception of the above-mentioned several natural populations, the tree trunks made the major contributions, 80–90%, to the total aboveground biomass inventories, while the contributions of branches and needles for a wide range of growing conditions in the ChEZ were rather accurately approximated by the negative power functions of M_{AG} (Supplementary materials, Fig. S6). Therefore, biomass inventories in compartments of typical Chernobyl pine stands can be derived from total aboveground biomass inventories as a $\times M_{AG}^{b}$ for M_{needle} and M_{branch} using the coefficients in the corresponding expressions shown in Fig. S6, and as M_{AG}-M_{needle}-M_{branch} for trunk.

Table 1
Biomass inventories in the aboveground compartments at the experimental sites.

Site ID	Origin of stand	M_{trunk} (kg m^{-2})		M_{needle} (kg m^{-2})		M_{branch} (kg m^{-2})		M_{AG} (kg m^{-2})	
		M	CI 0.95	M	CI 0.95	M	CI 0.95	M	CI 0.95
ChZ-1	Artificial	13.4	2.6	0.42	0.18	0.90	0.25	14.7	2.6
chz-1	Artificial	13.2	3.3	0.63	0.27	0.83	0.26	14.6	3.4
chz-2_2	Artificial	6.86	1.92	0.71	0.33	1.19	0.41	8.8	2.0
chz-2_3	Natural	0.37	0.19	0.07	0.05	0.16	0.10	0.59	0.22
chz-2_4	Natural	0.36	0.22	0.08	0.07	0.26	0.18	0.70	0.29
ChZ-3	Natural	11.0	2.1	0.28	0.13	0.92	0.35	12.2	2.2
ChZ-4	Artificial	17.7	4.8	0.53	0.28	1.21	0.48	19.4	4.8
ChZ-5	Artificial	15.7	3.5	0.56	0.23	0.82	0.26	17.0	3.6
ChZ-6	Artificial	8.24	1.96	0.56	0.24	0.77	0.24	9.6	2.0
ChZ-7	Artificial	8.09	2.13	0.54	0.24	0.65	0.22	9.3	2.2
ChZ-8	natural	7.16	1.35	0.34	0.17	0.81	0.33	8.3	1.4
chz-8	natural	7.76	2.33	0.36	0.18	0.89	0.37	9.0	2.4
chz-8_2	natural	0.86	0.35	0.11	0.07	0.42	0.22	1.4	0.4
ChZ-9	artificial	9.14	2.03	0.50	0.20	0.91	0.27	10.5	2.1
ChZ-10	artificial	4.78	1.14	0.52	0.23	0.80	0.26	6.1	1.2
ChZ-11	artificial	10.2	2.4	0.58	0.24	0.83	0.26	11.6	2.4
ChZ-12	artificial	13.1	2.8	0.65	0.26	0.79	0.23	14.5	2.8
ChZ-13	artificial	9.45	2.14	0.62	0.26	0.75	0.23	10.8	2.2
ChZ-14	artificial	18.2	3.9	0.68	0.28	0.89	0.27	19.8	3.9
ChZ-15	artificial	12.7	2.8	0.62	0.25	0.81	0.24	14.1	2.8
kopachy_1	natural	4.69	1.62	0.30	0.17	0.87	0.40	5.9	1.7
kopachy_2	natural	0.60	0.29	0.11	0.08	0.37	0.22	1.1	0.4
Rf	natural	0.12	0.08	0.05	0.04	0.23	0.17	0.40	0.19
FI-1	artificial	12.7	3.1	0.66	0.28	1.04	0.33	14.4	3.1
FI-2	natural	4.44	1.36	0.20	0.09	0.66	0.26	5.3	1.4
FI-3	natural	8.10	2.61	0.27	0.13	0.75	0.30	9.1	2.6
FI-4	natural	14.5	5.02	0.28	0.17	0.85	0.42	15.6	5.0
FI-5	natural	5.21	1.66	0.28	0.15	0.76	0.32	6.3	1.7
FI-6	artificial	14.5	3.8	0.63	0.28	1.14	0.38	16.2	3.8
FI-7	natural	2.49	0.82	0.24	0.15	0.63	0.31	3.4	0.9
FI-8	artificial	13.0	3.2	0.55	0.24	0.93	0.30	14.5	3.2
Summary									
AM		8.7		0.42		0.77		9.8	
Median		8.2		0.50		0.81		9.6	
STD		5.3		0.21		0.26		5.7	
CV		62		50		33		58	

Note: M_{trunk} is trunk biomass, M_{needle} is needle biomass, M_{branch} is crown branch biomass, M_{AG} is a total biomass of all aboveground compartments. M and CI 0.95 are mean and confidence interval at p-value = 0.05, respectively; AM is the arithmetic mean, STD is the standard deviation and CV is the coefficient of variation.

3.2. Estimates of biomass inventories in the CHM approach

The distributions of the CHM values obtained at each experimental plot are presented in Fig. 2. Artificial forest stands have rather high CHM values that are distributed within comparable narrow ranges due to the same age of trees in each plantation. The natural young populations consist of trees of different ages that germinated after the Chernobyl accident, which explains the greater variations in CHM values and lower mean and median values at these sites compared to the artificial stands.

Non-parametric analysis revealed correlations between the calculated statistical indices of CHM raster images (arithmetic mean, standard deviation, standard error, coefficient of variation, asymmetry, excess, sum, minimum and maximum, range, quantile ranges, percentiles etc.) and the aboveground biomass inventories at the studied sites calculated from the ground measurement results (Table 1). The strongest correlations with the aboveground biomass inventories at the sites were found for the arithmetic mean, coefficient of variation, and percentiles of CHM values in the corresponding raster images (Table 2).

M_{trunk} and M_{AG} in the studied forest stands correlated well with AM of CHM; moreover, the dependencies of these inventories on AM were very close in artificial and natural stands (Supplementary materials, Fig. S7). The strong correlations with AM were also found for M_{branch} and $M_{needles}$ in natural stands, whereas, there was no correlation for $M_{needles}$, and for M_{branch} the correlation was weak in artificial plantations. In the latter case, however, the inventories in natural and artificial plantations fit the same correlation dependence.

The compartment biomass inventories and the total aboveground biomass in natural stands also correlated with CV of CHM (Fig. S7). However, this parameter cannot be used to estimate biomass inventories in artificial plantations: the correlations with CV were weak for M_{trunk} and M_{AG} and absent for M_{branch} and $M_{needles}$. In addition, estimates of biomass inventories in natural forests based on CV deviated significantly from the actual inventories at low values of this parameter.

Despite of the fairly high pairwise correlation coefficients presented in Table 2, correlations between biomass inventories and CHM percentiles in artificial plantations were weak. In natural stands, correlations with M_{AG} occurred only for the higher percentiles (examples for M_{AG} are shown in Fig. S8 in Supplementary materials), and therefore these indices have limited predictive power for estimating biomass inventories.

Thus, among the analyzed CHM parameters, AM showed the greatest feasibility for use in UAV-based assessment of biomass inventories in pine forest stands in Chernobyl. For example, the simple linear dependencies on AM

$$M = a_0 + a_1 \cdot AM \quad (14)$$

can be successfully applied to estimate M_{AG} in both natural and artificial pine stands of different ages. The parameters of the dependence of M_{AG} on AM were determined at the whole set of the surveyed stands by the least-squares method: $a_0 = 0.96 \pm 0.95$ (estimate ± STD), $a_1 = 0.81 \pm 0.07$. Although the dependence was statistically significant according to Fisher's criteria ($F = 107$) at $p = 0.05$ ($F_{table} = 4.2$), the parameter a_0 was not significant (calculated Student's t-test value of 10.8 exceeded the tabulated value of 2.05). Therefore, the regression equation can be simplified to

$$M_{AG} = 0.874 \cdot AM \quad (15)$$

as shown in Fig. 3, with $R^2 = 0.79$ and root-mean-square error RMSE = 2.63 kg m^{-2}.

The utilization of the power function, as well as introduction of an additional independent variable, CV, into the regression equation (equations 22 and 23 in Table 3) does not result in a significant increase in the accuracy of the M_{AG} estimates compared to eq. (15). Biomass inventories in the stand compartments can be estimated using a linear (M_{trunk}) or power (all compartments) dependencies on AM of CHM (Table 3). Introduction of CV into the regression equations improves the accuracy of the estimate for only needle biomass (eq. 23) for which CV is a significant parameter at $p = 0.05$ (Table S2). M_{branch} can also be derived from the calculated value of M_{AG} (eq. 21) in the approach described in section 3.1; however, the accuracy of the M_{needle} estimate in this approach (eq. 24) is lower than that of the estimate based on CHM parameters.

Overall, the results obtained confirm the applicability of simple regressions using the basic statistical index of the CHM distributions, AM, to estimate aboveground biomass inventories in typical pine forest stands in the ChEZ without adjusting regression parameters depending

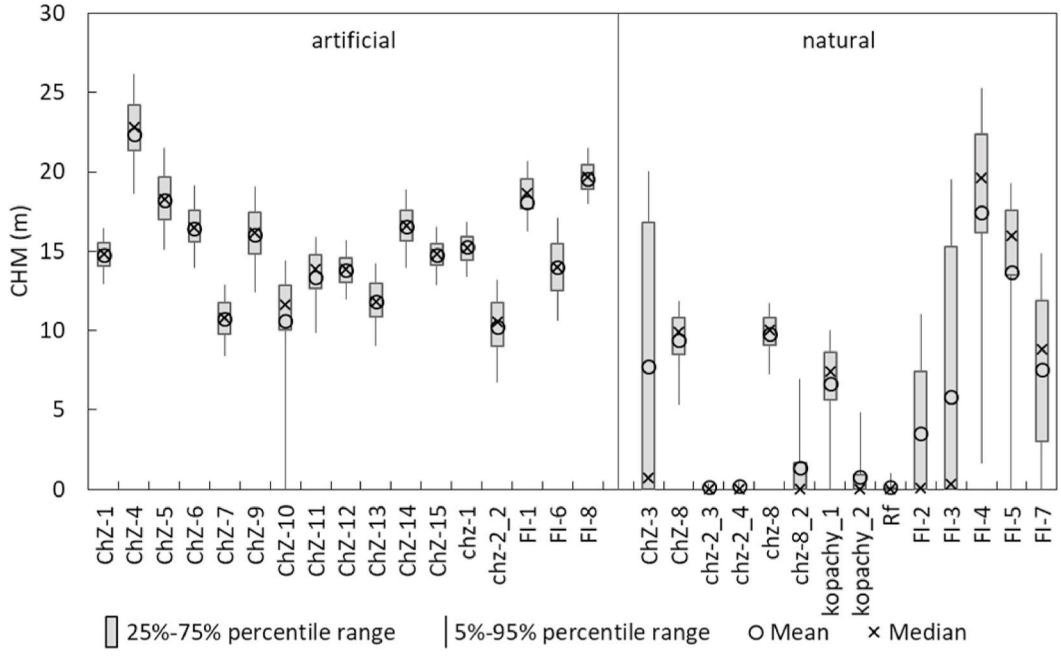

Fig. 2. Distributions of the CHM values at the experimental sites.

Table 2
Spearman's coefficients of pair correlations between statistical indices of the CHM distributions and the aboveground biomass inventories in the studied forest stands (critical $r_s = 0.36$ at p-value = 0.05).

Index	AM (m)	CV(%)	Percentile								
			1%	5%	10%	25%	50%	75%	90%	95%	99%
M_{trunk} (kg m^{-2})	0.87	−0.74	0.76	0.81	0.79	0.82	0.83	0.83	0.81	0.80	0.79
M_{needle} (kg m^{-2})	0.71	−0.84	0.80	0.77	0.80	0.69	0.67	0.52	0.47	0.45	0.42
M_{branch} (kg m^{-2})	0.67	−0.58	0.56	0.61	0.64	0.62	0.65	0.63	0.64	0.62	0.59
M_{AG} (kg m^{-2})	0.88	−0.75	0.77	0.82	0.80	0.82	0.83	0.82	0.80	0.79	0.78

Note: M_{trunk} is trunk biomass, M_{needle} is needle biomass, M_{branch} is crown branch biomass, M_{AG} is a total biomass of all aboveground compartments. AM is the arithmetic mean, and CV is the coefficient of variation.

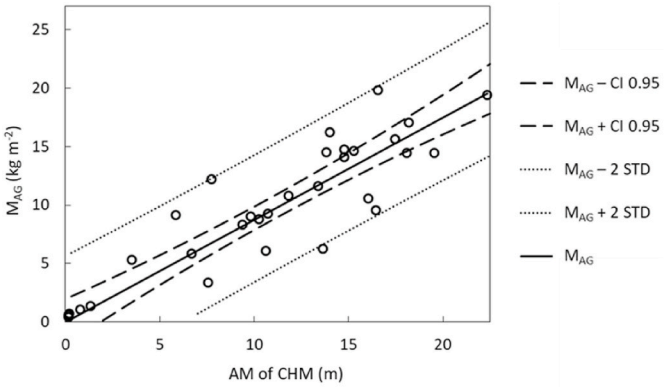

Fig. 3. Regression dependence for the total aboveground biomass inventory on AM in the CHM approach (eq. (15)), and confidence (±CI 0.95) and prognosis (±2 STD) intervals (p-value = 0.05).

Table 3
Regression equations for biomass inventory estimates in the CHM approach.

Equation		R^2	RMSE/RMSE (%)
(16)	$M_{trunk} = 0.778 \cdot AM$	0.78	2.52/29.1
(17)	$M_{trunk} = 0.957 \cdot AM^{0.924}$	0.78	2.51/29.0
(18)	$M_{trunk} = 1.274 \cdot AM^{0.865} \cdot CV^{-0.048}$	0.78	2.50/28.8
(19)	$M_{branch} = 0.423 \cdot AM^{0.280}$	0.76	0.13/16.4
(20)	$M_{branch} = 0.348 \cdot AM^{0.317} \cdot CV^{-0.035}$	0.76	0.12/16.2
(21)	$M_{branch} = 0.541 \cdot M_{AG}^{0.193}$ (artificial), $M_{branch} = 0.313 \cdot M_{AG}^{0.449}$ (natural)	0.76	0.12/16.2
(22)	$M_{needle} = 0.133 \cdot AM^{0.508}$	0.69	0.12/27.8
(23)	$M_{needle} = 0.578 \cdot AM^{0.207} \cdot CV^{-0.250}$	0.80	0.09/22.1
(24)	$M_{needle} = 0.498 \cdot M_{AG}^{0.06}$ (artificial), $M_{needle} = 0.096 \cdot M_{AG}^{0.514}$ (natural)	0.66	0.12/29.4
(25)	$M_{AG} = 0.874 \cdot AM$	0.79	2.63/26.7
(26)	$M_{AG} = 1.356 \cdot AM^{0.838}$	0.80	2.57/26.2
(27)	$M_{AG} = 1.843 \cdot AM^{0.774} \cdot CV^{-0.051}$	0.80	2.55/25.9

Note: M_{trunk} is trunk biomass, M_{needle} is needles biomass, M_{branch} is crown branch biomass, M_{AG} is a total biomass of all aboveground compartments (all inventories are in kg m^{-2}). AM is the arithmetic mean of CHM (m). CV is the coefficient of variation of CHM (%). RMSE is the root mean square error of predicted inventory value (kg m^{-2}). R^2 and RMSE are calculated relatively to the inventory values obtained from ground-based measurements.

on age, origin, stand density, etc., which allows to use the CHM approach for UAV surveys of forests in this area. The regressions shown in Table 3 explain up to 80% of the variation in aboveground biomass inventories. Close ranges of R^2 values were reported in other studies where aboveground biomass inventories in variety of the local conditions were calculated based on certain indices derived from CHM: 0.65–0.87 in boreal and temperate forest stands in the USA (Lefsky at al., 2002); 0.74 in coniferous forest in China (He et al., 2013); 0.79–0.94 in seasonal tropical forests in Cambodia (Ota et al., 2015); 0.81–0.83 in tropical forests in Costa Rica (Zahawi et al., 2015); up to 0.67 in tropical woodlands in Malawi (Kachamba et al., 2016); up to 0.86 in tropical monoculture plantations in Panama (Miller et al., 2017); 0.78–0.94 in mixed uneven-aged forests in Japan (Jayathunga et al., 2019), etc. The cited studies were performed over two decades using different equipment (digital photography and LIDAR) and software, and different CHM metrics as explanatory variables; however, the accuracy of the aboveground biomass estimates did not differ significantly between the studies. The accuracies of CHM were influenced by various factors. For example, unlike LIDAR surveys, photogrammetric methods cannot provide an accurate DEM and, respectively, an accurate CHM for dense forests growing in hilly terrains (Cao et al., 2019; Guimarães et al., 2020); smaller trees can be shaded by taller ones and therefore will not be accounted for in the CHM distribution, while in fact they do contribute to the total stand biomass, etc.

On the other hand, we compare the biomass inventory estimates from airborne measurements with those obtained from field measurements of DBH and H from using eqs. (1)–(6) under the assumption that the latter are "true" inventories. However, the most accurate ground-based method for biomass estimates implies cutting model trees (Anuchin, 1982; van Laar and Akça, 2007). The above equations provide reasonably accurate estimates of inventories in artificial overstocked stands, where the relative deviations of predicted values from actual aboveground biomass inventories are within 10%. The accuracy of estimates decreases sharply with decreasing stand density and tree size, mainly because of the increase and large variation in the contribution of crown compartments into total above-ground biomass (Schepaschenko et al., 2008).

An analysis of the effect of some stand parameters on the deviation between aerial and ground-based estimates of biomass inventories is presented in section 4.

3.3. Estimates of biomass inventories in the ITD approach

Identification of individual trees at the CHM raster images was performed using the approach described in 2.3.2. The values of r_n obtained in the artificial (denser) stands are smaller than in the natural stands (Supplementary materials, Fig. S9). We derived the following dependencies of r_F on average tree height

$$r_F(H) = 0.115\ H + 1.31 \quad (28)$$

in natural stands, and

$$r_F(H) = 0.057\ H + 0.841 \quad (29)$$

in artificial plantations.

The individual tree detection efficiency data are shown in Fig. S10 (Supplementary materials). Detection ratios were higher in artificial plantations, ranging from 0.28 to 0.83 (mean 0.46) versus 0.16 to 0.66 (mean 0.38) in natural stands. In both artificial and natural stands, detection ratios decreased with increasing plantation density (number of trees per unit area). Fig. S11 in Supplementary materials illustrates the effect of heterogeneous spatial distribution of trees on detection efficiency: in dense groups, only the highest local maxima were recognized as individual trees, as other maxima were located at distances shorter

than r_F obtained for the highest maxima using the expression for natural stands (eq. (28)).

The average heights of the detected trees correlated well with the results of their ground-based measurements in artificial stands (Fig. 4). The ratios between average heights estimated in the ITD approach and those obtained in ground-based measurements in artificial stands were very close to unity, with a mean of 0.97 and STD = 0.11 ($R^2 = 0.74$). The correlation was weaker in natural stands, as well as the accuracy of the ITD approach was lower, showing a mean ratio of average stand heights of 0.88 at STD = 0.34 ($R^2 = 0.63$). The largest deviations of estimated average heights from their values obtained in field measurements occurred in natural stands with the lowest tree detection ratios. Values of R^2 in our study were close to those reported for the tree height estimates using UAV imagery, 0.68 to 0.75 (Panagiotidis et al. (2017); Wallace et al. (2016)); use of LIDAR increased the accuracy of the tree height estimates ($R^2 = 0.84$ in Wallace et al. (2016)).

Among other tested parameters, non-parametric analysis revealed significant correlations ($r_s > 0.5$ at $p = 0.05$) only between the aboveground tree biomass inventory components in the studied stands and the total crown projection areas and mean and median tree heights derived from CHM in the ITD approach (Table 4). However, the total crown projection areas correlate well with mean heights ($r_s = 0.49$), which limits the simultaneous use of both indicators in the regression equations.

The total aboveground biomass inventories in the studied stands increased with average height of the detected trees and with the total crown projection areas (Supplementary materials, Fig. S12 a, b); however, a stronger correlation was found between the total biomass inventories and the product of the power functions of both of these parameters, $aH^x p_{crown}^y$, with the coefficients *a, x* and *y* given in Table 5 (eq. 33). Moreover, in this case the biomass inventories in both artificial and natural stands could be described by the same regression relationship (Supplementary materials, Fig. S12 c). The same regression dependencies for artificial and natural stands could also be used to estimate the biomass compartment inventories (eqs. 30–32, respectively; Fig. S12 d, e); however, in natural stands, the needle biomass inventory may be underestimated (regression coefficient is 0.7). It should also be noted that the average tree height is a more significant parameter than the total crown projection area for predicting M_{trunk}, M_{branch} and M_{AG} (eqs. 30, 31 and 33 in Table S2) whereas this parameter is not significant in the regression equation for needles at $p = 0.05$ (eq. 32).

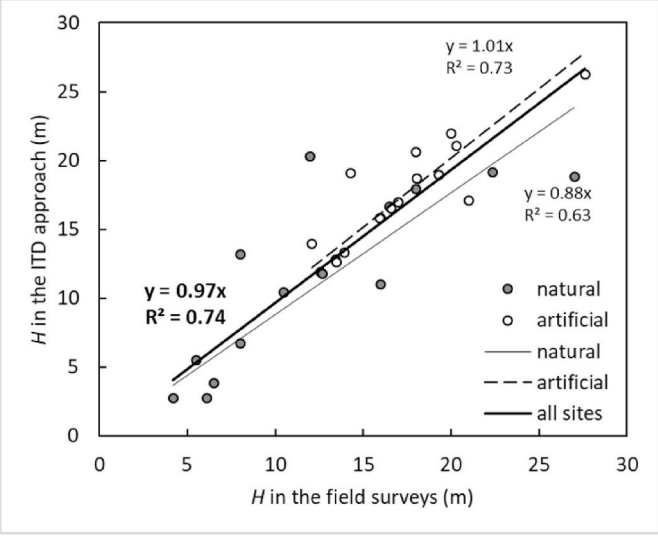

Fig. 4. Average tree heights derived from the CHM of the studied stands using the ITD approach vs average stand heights measured in the field surveys.

The accuracy of estimate of the total aboveground biomass in typical pine stands in Chernobyl obtained in the ITD approach using eq. 33 is illustrated in Fig. 5. The coefficients of determination varied from 0.74 for needles to 0.78 for total aboveground biomass (Table 5), which is within the range of R^2 values of 0.63–0.96 reported in other studies for aboveground biomass inventory estimates derived from parameters of individual trees detected at CHM (Lin J. et al., 2018; Guimarães, N. et al., 2020; Navarro F. et al., 2020). The accuracy of the ITD approach can be impacted by a number of factors such as flight altitude, distance between UAV tracks, weather conditions, landscape, etc.

4. Discussion

In this study, we analyzed the applicability of UAV-based surveys for assessment of the aboveground biomass inventories in typical Scots pine forests of various ages and origins in the Chernobyl Exclusion Zone. We applied two different approaches to processing of photogrammetric data. In the CHM approach, as in other studies (Lefsky at al., 2002; He et al., 2013; Ota et al., 2015; Zahawi et al., 2015; Kachamba et al., 2016; Goodbody et al., 2017a, b; Miller et al., 2017; Iglhaut et al., 2019; Guimarães et al., 2020; Kotivuori et al., 2020; Zhao et al., 2020), we aimed to establish correlations between the CHM distribution parameters and the aboveground tree biomass inventories in the studied forest stands. We found that at our sites, the inventories could be most accurately predicted based on the arithmetic means of CHM (Fig. 3; eq. (15)). In the ITD approach, we determined the heights of individual trees detected at CHM and then derived the biomass inventories based on average tree heights at the sites. We found that due to the high density of stands and especially its substantial variability within the site areas, only a part of all trees at the study sites could be detected, however, the mean heights of the trees detected corresponded well to the mean heights of the trees in the studied stands measured in the field. Successful identification of tree indices in closed stands has been reported in a limited number of publications (Alonzo et al., 2018; Guimarães, 2020), while higher detection accuracy of individual trees has been achieved in low-grade groups of separated trees and shrubs (e.g. Mohan et al., 2017; Lin et al., 2018; Yan et al., 2020). The accuracy of individual tree detection can improve if CHM is analyzed along with RGB or near-infrared remote sensing data (Osco et al., 2020; Xu et al., 2019). However, we found that heights of only a part of all trees in the studied stand along with data on total tree projections areas might be sufficient to predict the biomass inventory (Fig. 5; eq. 33).

Overall, the two approaches provide very close estimates of the aboveground biomass inventories at the study sites (Supplementary materials, Fig. S13) although the ITD approach predicts slightly higher values than the CHM approach for natural populations. This may be due to the predominant detection of higher trees in dense parts of the stand arising from the application of the filtering procedure.

Given the large variations in the studied forest stand parameters (Supplementary materials, Table S1), one could expect the accuracy of the biomass estimates derived from UAV-survey data to vary from site to site. For instance, in the introduction, we assumed the potential influence of morphological anomalies on the accuracy of biomass estimates. The proportion of abnormal trees *AT* ranged from 3.3% at the site ChZ-1 to 76.2% at the site Rf. Higher values of *AT* were found at the sites with smaller total crown projections areas p_{crown}, whereas in dense populations *AT* was mostly less than 20% (Supplementary materials, Fig. S14), which follows from general patterns of individual tree development in forest stands (Trouvé et al., 2015). Unlike the other stand parameters (*AT*, *RS*, *D*), p_{crown} is a parameter that can be directly derived from the UAV-survey data (CHM). Fig. 6 shows the effect of this parameter on the accuracy of the biomass inventory estimates obtained with the two approaches applied in this study. Here, we considered the aboveground biomass inventory estimates from ground-based observations, M_{AGgb}, as "true" inventories, and analyzed the relative deviations $\Delta M_{AG}/M_{AGgb}$, ($\Delta M_{AG} = M_{AGCHM} - M_{AGgb}$ and $\Delta M_{AG} = M_{AGITD} - M_{AGgb}$) of

Table 4
Spearman's coefficients of pair correlations between parameters of detected individual trees and the aboveground biomass inventories in the studied forest stands (critical $r_s = 0.36$ at p-value = 0.05).

Index	p_{crown}	Heights of the detected trees (m)					Crown area (m^2)					$N_{treetop}$
		AM	Median	STD	min	max	AM	Median	STD	min	max	
M_{trunk} (kg m^{-2})	0.73	0.79	0.79	−0.21	0.57	0.77	0.22	0.28	0.05	0.13	0.09	0.55
M_{needle} (kg m^{-2})	0.76	0.51	0.44	−0.43	0.69	0.38	−0.01	0.08	−0.20	0.21	−0.12	0.58
M_{branch} (kg m^{-2})	0.68	0.63	0.62	−0.24	0.42	0.58	0.45	0.51	0.30	0.14	0.32	0.54
M_{AG} (kg m^{-2})	0.73	0.79	0.79	−0.21	0.56	0.77	0.22	0.28	0.05	0.13	0.09	0.56

Note: M_{trunk} is trunk biomass, M_{needle} is needle biomass, M_{branch} is crown branch biomass, M_{AG} is a total biomass of all aboveground compartments (all inventories are in kg m^{-2}). $N_{treetop}$ is a number of detected trees per unit area, AM is the arithmetic mean, STD is the standard deviation, p_{crown} is the total crown projection area.

Table 5
Regression equations for biomass inventory estimates in the ITD approach.

Equation		R^2	RMSE/RMSE (%)
30	$M_{trunk} = 0.524 \cdot H^{1.079} \cdot p_{crown}^{0.762}$	0.76	2.61/30.2
31	$M_{branch} = 0.402 \cdot H^{0.283} \cdot p_{crown}^{0.313}$	0.77	0.12/15.7
32	$M_{needle} = 0.328 \cdot H^{0.177} \cdot p_{crown}^{1.292}$	0.74	0.11/25.5
33	$M_{AG} = 0.768 \cdot H^{0.987} \cdot p_{crown}^{0.722}$	0.78	2.68/27.2

Note: M_{trunk} is trunk biomass, M_{needle} is needles biomass, M_{branch} is crown branch biomass, M_{AG} is a total biomass of all aboveground compartments (all inventories are in kg m^{-2}). H is the arithmetic mean of heights of the detected trees (m). p_{crown} is the total crown projection area. RMSE is the root mean square error of the predicted inventory value (kg m^{-2}). R^2 and RMSE are calculated relatively to the inventory values obtained from ground-based measurements.

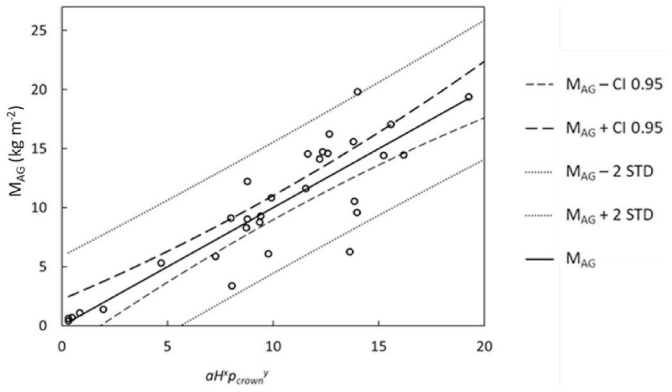

Fig. 5. Regression dependence of total aboveground biomass inventory in the ITD approach (eq. 33), and confidence (±CI 0.95) and prognosis (±2 STD) intervals (p-value = 0.05).

the aboveground biomass estimates as function of p_{crown}. With p_{crown} values close to 1, the accuracy of the biomass inventory estimates did not differ between the two approaches and was adequate for tasks related to radioecological monitoring in the Chernobyl Exclusion Zone: the average $\Delta M_{AG}/M_{AGgb}$ in this group of stands were close to 0 and STD did not exceed 0.2, while the STD of radionuclide activity concentrations measured in the same biomass compartment within the same forest stand are usually larger (e.g., Yoschenko et al., 2006; Holiaka et al., 2020b, 2020c) and thus concentration variations would contribute major uncertainties in determining the radionuclide distributions in forest ecosystems. The results of the biomass inventory estimates based on the UAV-survey data in stands with low p_{crown} deviated significantly from those derived from ground-based measurements (Fig. 6). In all groups of the low p_{crown} stands, the estimates obtained in the ITD approach were higher than in the CHM approach. In general, since the low p_{crown} values obtained from CHM were associated with low reliability of the aboveground biomass estimates in both approaches, p_{crown} can be seen as a principal parameter limiting the use of UAV surveys for assessment of the biomass inventories. At high p_{crown} values (two groups

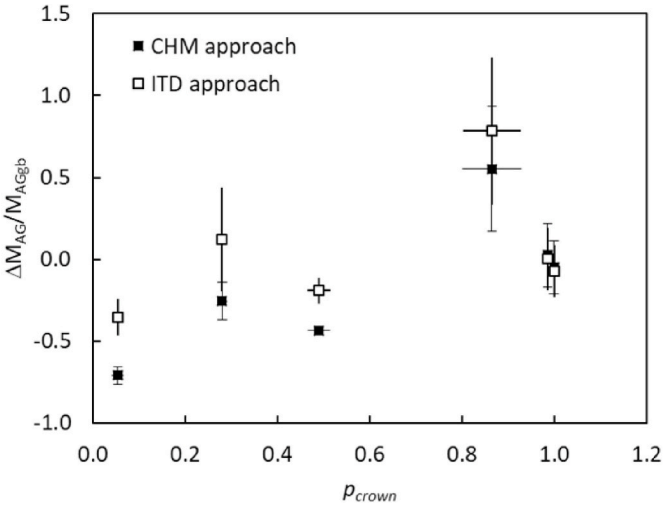

Fig. 6. Accuracy of the aboveground biomass inventory estimates in the UAV-surveys vs the total crown projections areas. The vertical and horizontal bars represent the STD of the parameters in the groups of stands.

of stands with p_{crown} >0.98 in Fig. 6), variations in other stand parameters show no effect on the accuracy of biomass inventory estimates (Supplementary materials, Fig. S15).

Overall, our study demonstrated the applicability and limitations of the CHM and ITD approaches to the UAV survey data processing for assessment of the aboveground biomass inventories in typical pine forests in the Chernobyl Exclusion Zone. The results of statistical analysis (Supplementary materials, Table S2) confirmed the validity of the obtained regression dependencies for the estimation of aboveground biomass inventories for a wide range of local conditions (stand age, stand density, height of trees, etc.) in the study area. The general approach developed in the study can be used to calibrate the UAV-based biomass assessment methods for other forest conditions, such as those at Fukushima or in areas that can be affected by hypothetical major nuclear reactor accidents (Engler, 2020).

5. Conclusions

Our study demonstrated the applicability and limitations of UAV surveys for large-scale monitoring of aboveground biomass inventories in typical radioactive contaminated Scots pine forests of the Chernobyl Exclusion Zone, where ground-based surveys would result in radiation exposure of personnel. We calibrated two approaches used in UAV surveys to photogrammetric data processing, and compared their accuracy with ground-based measurements at 31 experimental sites that differed in local conditions (origin, age, plantation density, presence of abnormal trees etc.). Applying these approaches requires determining the parameters to be derived from photogrammetric data that will provide the most accurate estimates of biomass for specific conditions in the study area. We found that the total aboveground biomass inventories

correlated well ($R^2 = 0.79$) with the mean CHM value of the site (CHM approach) and with the average height of trees detected on the site and the total crown projection area ($R^2 = 0.78$; ITD approach). Based on this, we established dependencies to estimate trunk, branch, needle and total biomass inventories using these parameters. The accuracy of the aboveground biomass inventory estimates based on the UAV survey data in both approaches was high in stands with high total crown projections areas (>0.90). Accordingly, these approaches can be successfully applied in radioecological monitoring to assess the inventories and dynamics of incorporated artificial radionuclides (particularly, ^{90}Sr and ^{137}Cs) in the forest biomass of dense overstocked stands, which are typical for the ChEZ due to lack of proper forest maintenance. Both approaches demonstrated lower performance in forests formed by separated groups of uneven-aged (mostly young) trees.

Currently, radioactively contaminated ChEZ lands in Ukraine and Belarus are part of nature reserves. According to the national legislations, their functions are to prevent the spread of radionuclides to neighboring territories (including transboundary transportation), to preserve biodiversity, and to serve as observatories for studying the cycles of radionuclides in the environment and their impact on biota. Application of the remote sensing approaches developed in this study, and their further improvement, are well in line with these functions. First, they allow to perform radioecological monitoring and forest inventory surveys using rather inexpensive tools under conditions where the personnel exposures are strictly regulated by national hygienic norms. Second, such surveys can cover areas that are difficult to access. Finally, the use of UAVs instead of ground-based forest survey expeditions allows less disturbance to wild animals inhabiting forest ecosystems.

From the perspective of radioecological monitoring and forest management in the ChEZ, future efforts should include the elaboration of approaches for more accurate biomass estimation in uneven-aged pine stands as well as in broadleaved and mixed forests. The general approach developed in the study could also be used to calibrate UAV-based biomass assessment methods in other forest conditions.

CRediT statement

Dmytrii Holiaka: Investigation, Software, Formal analysis, Methodology, Writing and Revision, Visualization. **Hiroaki Kato:** Conceptualization, Methodology, Validation, Writing – Reviewing. **Vasyl Yoschenko:** Conceptualization, Methodology, Investigation, Formal analysis, Writing and Revision, Supervision. **Yuichi Onda:** Conceptualization, Supervision, Methodology, Investigation, Writing – Reviewing. **Yasunori Igarashi:** Methodology, Investigation, Resources, Writing – Reviewing and Editing. **Kenji Nanba:** Funding acquisition, Project administration, Writing – Reviewing. **Petro Diachuk:** Investigation. **Maryna Holiaka:** Investigation. **Roman Zadorozhniuk:** Investigation. **Valery Kashparov:** Project administration, Resources, Writing – Reviewing. **Ihor Chyzhevskyi:** Resources, Writing – Reviewing.

Declaration of competing interest

The authors declare that they have no known competing financial interests or personal relationships that could have appeared to influence the work reported in this paper.

Acknowledgements

This work was supported by JST and JICA through the Japanese government program for international joint research into global issues entitled the Science and Technology Research Partnership for Sustainable Development (SATREPS; grant number JPMJSA1603 “The Project for Strengthening of the Environmental Remediation of Radioactively Contaminated Sites”), and by Environmental Radioactivity Research Network Center (ERAN; grant number: Y-19-01 “Estimation of Biomass and Stocks Biologically Mobility Radionuclides Using Methods of Processing Aboveground and Remote Sensing Data for Radioactively Contaminated Forests in Ukraine”). The authors express sincere gratitude to Mr. Serhii Kirieiev (SSE Ecocentre), Dr. Shinichiro Uematsu (former CRIED), and Ms. Hiroko Nagata and Mr. Hiroshi Kataoka (IER) for their assistance in organizing and conducting the research.

Appendix A. Supplementary data

Supplementary data to this article can be found online at https://doi.org/10.1016/j.jenvman.2021.113319.

References

Abdollahnejad, A., Panagiotidis, D., Surový, P., 2018. Estimation and extrapolation of tree parameters using spectral correlation between UAV and Pléiades data. Forests 9, 85. https://doi.org/10.3390/f9020085.

Ager, A.A., Lasko, R., Myroniuk, V., Zibtsev, S., Day, M.A., Usenia, U., Bogomolov, V., Kovalets, I., Evers, C.R., 2019. The wildfire problem in areas contaminated by the Chernobyl disaster. Sci. Total Environ. 696, 133954. https://doi.org/10.1016/j.scitotenv.2019.133954.

Alonzo, M., Andersen, H.E., Morton, D., Cook, B., 2018. Quantifying boreal forest structure and composition using UAV structure from motion. Forests 9, 119. https://doi.org/10.3390/f9030119.

Anuchin, N., 1982. Forest Mensuration. Forest industry, Moscow (in Russian).

Brovkina, O., Cienciala, E., Surový, P., Janata, P., 2018. Unmanned aerial vehicles, UAV) for assessment of qualitative classification of Norway spruce in temperate forest stands. Geo Spatial Inf. Sci. 21 (1), 12–20. https://doi.org/10.1080/10095020.2017.1416994.

Cao, L., Liu, H., Fu, X., Zhang, Z., Shen, X., Ruan, H., 2019. Comparison of UAV LiDAR and digital aerial photogrammetry point clouds for estimating forest structural attributes in subtropical planted forests. Forests 10, 145. https://doi.org/10.3390/f10020145.

Cruzan, M.B., Weinstein, B.G., Grasty, M.R., Kohrn, B.F., Hendrickson, E.C., Arredondo, T.M., Thompson, P.G., 2016. Small unmanned aerial vehicles (micro-UAVs, drones) in plant ecology. Appl. Plant Sci. 4, 9. https://doi.org/10.3732/apps.1600041.

Engler, J.-O., 2020. Global and regional probabilities of major nuclear reactor accidents. J. Environ. Manag. 269, 110780. https://doi.org/10.1016/j.jenvman.2020.110780.

Evangeliou, N., Balkanski, Y., Cozic, A., Hao, W.M., Møller, A.P., 2014. Wildfires in Chernobyl-contaminated forests and risks to the population and the environment: a new nuclear disaster about to happen? Environ. Int. 73, 346–358. https://doi.org/10.1016/j.envint.2014.08.012.

Evangeliou, N., Zibtsev, S., Myroniuk, V., Zhurba, M., Hamburger, T., Stohl, A., Balkanski, Y., Paugam, R., Mousseau, T.A., Møller, A.P., Kireev, S.I., 2016. Resuspension and atmospheric transport of radionuclides due to wildfires near the Chernobyl Nuclear Power Plant in 2015: an impact assessment. Sci. Rep. 6, 26062. https://doi.org/10.1038/srep26062.

Eysn, L., Hollaus, M., Lindberg, E., Berger, F., Monnet, J.-M., Dalponte, M., Kobal, M., Pellegrini, M., Lingua, E., Mongus, D., Pfeifer, N., 2015. A benchmark of lidar-based single tree detection methods using heterogeneous forest data from the alpine space. Forests 6, 1721–1747. https://doi.org/10.3390/f6051721.

Giannetti, F., Chirici, G., Gobakken, T., Naesset, E., Travaglini, D., Puliti, S., 2018. A new approach with DTM-independent metrics for forest growing stock prediction using UAV photogrammetric data. Remote Sens. Environ. 213, 195–205. https://doi.org/10.1016/j.rse.2018.05.016.

Goodbody, T., Coops, N., Marshall, P., Tompalski, P., Crawford, P., 2017a. Unmanned aerial systems for precision forest inventory purposes: a review and case study. For. Chron. 93 (1), 71–81. https://doi.org/10.5558/tfc2017-012.

Goodbody, T., Coops, N., Tompalski, P., Crawford, P., Day, K., 2017b. Updating residual stem volume estimates using ALS- and UAV-acquired stereo-photogrammetric point clouds. Int. J. Rem. Sens. 38, 8–10. https://doi.org/10.1080/01431161.2016.1219425.

Goor, F., Thiry, Y., Delvaux, B., 2007. Radiocaesium accumulation in stem wood: integrated approach at the scale of forest stands for contaminated Scots pine in Belarus. J. Environ. Manag. 85, 129–136. https://doi.org/10.1016/j.jenvman.2006.08.008.

Guimarães, N., Pádua, L., Marques, P., Silva, N., Peres, E., Sousa, J.J., 2020. Forestry remote sensing from unmanned aerial vehicles: a review focusing on the data, processing and potentialities. Rem. Sens. 12, 1046. https://doi.org/10.3390/rs12061046.

He, Q., Chen, E., An, R., Li, Y., 2013. Above-ground biomass and biomass components estimation using LiDAR data in a coniferous forest. Forests 4, 984–1002. https://doi.org/10.3390/f4040984.

Holiaka, D., Kato, H., Yoschenko, V., Igarashi, Y., Onda, Y., Avramchuk, O., Holiaka, M., Humenyuk, V., Lesnyk, O., 2018. Identification and estimation of heights of Scots pine trees in forest stands in the Chernobyl exclusion zone using stereophotogrammetry method. Sci. Bullet. UNFU 28 (10), 18–21. https://doi.org/10.15421/40281003 (in Ukrainian).

Holiaka, D., Levchuk, S., Kashparov, V., Holiaka, M., Yoschenko, L., Otreshko, L., Kosarchuk, O., Lazarev, N., 2020a. Vertical distribution of ^{90}Sr in soil profiles and its uptake by Scots pine (*Pinus sylvestris* L.) wood growing within the Chernobyl

exclusion zone. Nucl. Phys. Atomic Energy 21, 157–165. https://doi.org/10.15407/jnpae2020.02.157 (in Ukrainian).
Holiaka, D., Levchuk, S., Yoschenko, V., Kashparov, V., Yoschenko, L., Holiaka, M., Pavliuchenko, V., Diachuk, P., Zadorozhniuk, R., Morozova, V., 2020b. ^{90}Sr and ^{137}Cs inventories in the depots and biogenic fluxes of the typical forest stands in the Chernobyl exclusion zone. Nucl. Phys. Atomic Energy 21, 256–264. https://doi.org/10.15407/jnpae2020.03.256 (in Ukrainian).
Holiaka, D., Yoschenko, V., Levchuk, S., Kashparov, V., 2020c. Distributions of ^{137}Cs and ^{90}Sr activity concentrations in trunk of Scots pine (*Pinus sylvestris* L.) in the Chernobyl zone. J. Environ. Radioact. 222, 106319. https://doi.org/10.1016/j.jenvrad.2020.106319.
Huylenbroeck, L., Laslier, M., Dufour, S., Georges, B., Lejeune, P., Michez, A., 2020. Using remote sensing to characterize riparian vegetation: a review of available tools and perspectives for managers. J. Environ. Manag. 267, 110652. https://doi.org/10.1016/j.jenvman.2020.110652.
Igarashi, Y., Onda, Y., Wakiyama, Y., Konoplev, A., Zheleznyak, M., Lisovyi, H., Laptev, G., Damiyanovich, V., Samoilov, D., Nanba, K., Kirieiev, S., 2020. Impact of wildfire on ^{137}Cs and ^{90}Sr wash-off in heavily contaminated forests in the Chernobyl exclusion zone. Environ. Pollut. 259, 113764. https://doi.org/10.1016/j.envpol.2019.113764.
Iglhaut, J., Cabo, C., Puliti, S., Piermattei, L., O'Connor, J., Rosette, J., 2019. Structure from motion photogrammetry in forestry: a review. Curr. For. Rep. 5, 155–168. https://doi.org/10.1007/s40725-019-00094-3.
Jayathunga, S., Owari, T., Tsuyuki, S., 2019. Digital aerial photogrammetry for uneven-aged forest management: assessing the potential to reconstruct canopy structure and estimate living biomass. Rem. Sens. 11, 338. https://doi.org/10.3390/rs11030338.
Kachamba, D.J., Ørka, H.O., Gobakken, T., Eid, T., Mwase, W., 2016. Biomass estimation using 3D data from unmanned aerial vehicle imagery in a tropical woodland. Rem. Sens. 8, 968. https://doi.org/10.3390/rs8110968.
Kangas, A., Maltamo, M., 2006. Forest Inventory. Methodology and Applications. Springer, Dordrecht. https://www.springer.com/gp/book/9781402043796.
Kashparov, V.A., Lundin, S.M., Kadygrib, A.M., Protsak, V.P., Levtchuk, S.E., Yoschenko, V.I., Kashpur, V.A., Talerko, N.M., 2000. Forest fires in the territory contaminated as a result of the Chernobyl accident: radioactive aerosol resuspension and exposure of fire-fighters. J. Environ. Radioact. 51, 281–298. https://doi.org/10.1016/S0265-931X(00)00082-5.
Kashparov, V.A., Lundin, S.M., Zvarych, S.I., Yoshchenko, V.I., Levchuk, S.E., Khomutinin, Y.V., Maloshtan, I.M., Protsak, V.P., 2003. Territory contamination with the radionuclides representing the fuel component of Chernobyl fallout. Sci. Total Environ. 317, 105–119. https://doi.org/10.1016/S0048-9697(03)00336-X.
Kashparov, V.A., Myroniuk, V.V., Zhurba, M.A., Zibtsev, S.V., Glukhovskiy, A.S., Zhukova, O.M., 2017. Radiological consequences of the fire in the Chernobyl exclusion zone in April 2015. Radiation biology. Radioecology 57 (5), 512–527.
Kashparov, V., Levchuk, S., Zhurba, M., Protsak, V., Khomutinin, Y., Beresford, N.A., Chaplow, J.S., 2018. Spatial datasets of radionuclide contamination in the Ukrainian Chernobyl exclusion zone. Earth Syst. Sci. Data 10, 339–353. https://doi.org/10.5194/essd-10-339-2018.
Kashparov, V., Levchuk, S., Zhurba, M., Protsak, V., Beresford, N.A., Chaplow, J.S., 2020. Spatial radionuclide deposition data from the 60 km radial area around the Chernobyl Nuclear Power Plant: results from a sampling survey in 1987. Earth Syst. Sci. Data 12, 1861–1875. https://doi.org/10.5194/essd-12-1861-2020.
Kashpor, S., Strochinskii, A., 2013. Forest stand parameters handbook. Vynychenko, Kyiv (in Ukrainian).
Keefe, R.F., Wempe, A.M., Becker, R.M., Zimbelman, E.G., Nagler, E.S., Gilbert, S.L., Caudill, C.C., 2019. Positioning methods and the use of location and activity data in forests. Forests 10, 458. https://doi.org/10.3390/f10050458.
Kotivuori, E., Kukkonen, M., Mehtätalo, L., Maltamo, M., Korhonen, L., Packalen, P., 2020. Forest inventories for small areas using drone imagery without in-situ field measurements. Remote Sens. Environ. 237, 111404. https://doi.org/10.1016/j.rse.2019.111404.
Kuželka, K., Slavík, M., Surový, P., 2020. Very high density point clouds from UAV laser scanning for automatic tree stem detection and direct diameter measurement. Rem. Sens. 12, 1236. https://doi.org/10.3390/rs12081236.
Lakida, P., Havryshenko, V., Korsun-Shevchenkivskyi, 2013. Standards for Assessment of Aboveground Phytomass of Stand Components of the Main Forest-Forming Tree Species of Ukraine (in Ukrainian).
Lefsky, M.A., Cohen, W.B., Harding, D.J., Parker, G.G., Acker, S.A., Gower, S.T., 2002. Lidar remote sensing of above-ground biomass in three biomes. Global Ecol. Biogeogr. 11, 393–399. https://doi.org/10.1046/j.1466-822x.2002.00303.x.
Li, W., Guo, Q., Jakubowski, M.K., Kelly, M., 2012. A new method for segmenting individual trees from the lidar point cloud. Photogramm. Eng. Rem. Sens. 78 (1), 75–84. https://doi.org/10.14358/PERS.78.1.75.
Lin, J., Wang, M., Ma, M., Lin, Y., 2018. Aboveground tree biomass estimation of sparse subalpine coniferous forest with UAV oblique photography. Rem. Sens. 10 (11), 1849. https://doi.org/10.3390/rs10111849.
Miller, E., Dandois, J.P., Detto, M., Hall, J.S., 2017. Drones as a tool for monoculture plantation assessment in the steep land tropics. Forests 8, 168. https://doi.org/10.3390/f8050168.
Mohan, M., Silva, C.A., Klauberg, C., Jat, P., Catts, G., Cardil, A., Hudak, A.T., Dia, M., 2017. Individual tree detection from unmanned aerial vehicle (UAV) derived canopy height model in an open canopy mixed conifer forest. Forests 8, 340. https://doi.org/10.3390/f8090340.
Navarro, A., Young, M., Allan, B., Carnell, P., Macreadie, P., 2020. The application of Unmanned Aerial Vehicles (UAVs) to estimate above-ground biomass of mangrove ecosystems. Rem. Sens. Environ. 242, 111747. https://doi.org/10.1016/j.rse.2020.111747.
Nikonchuk, V., 2015. Report for the round table "Exclusion zone: present and future" at SAUEZM on 13.11.2015 (in Ukrainian). http://dazv.gov.ua/images/presentacii/Nikonchuk%20-%202015.11.13.pdf. (Accessed 9 March 2021).
Osco, L.P., Arruda, M., dos, S. de, Marcato Junior, J., da Silva, N.B., Ramos, A.P.M., Moryia, É.A.S., Imai, N.N., Pereira, D.R., Creste, J.E., Matsubara, E.T., Li, J., Gonçalves, W.N., 2020. A convolutional neural network approach for counting and geolocating citrus-trees in UAV multispectral imagery. ISPRS J. Photogramm. 160, 97–106. https://doi.org/10.1016/j.isprsjprs.2019.12.010.
Ota, T., Ogawa, M., Shimizu, K., Kajisa, T., Mizoue, N., Yoshida, S., Takao, G., Hirata, Y., Furuya, N., Sano, T., Sokh, H., Ma, V., Ito, E., Toriyama, J., Monda, Y., Saito, H., Kiyono, Y., Chann, S., Ket, N., 2015. Aboveground biomass estimation using structure from motion approach with aerial photographs in a seasonal tropical forest. Forests 6, 3882–3898. https://doi.org/10.3390/f6113882.
Otero, V., Kerchove, R., Satyanarayana, B., Martínez-Espinosa, C., Fisol, M., Ibrahim, M., Sulong, I., Mohd-Lokman, H., Lucas, R., Dahdouh-Guebas, F., 2018. Managing mangrove forests from the sky: forest inventory using field data and Unmanned Aerial Vehicle, UAV) imagery in the Matang Mangrove Forest Reserve, peninsular Malaysia. For. Ecol. Manag. 411, 35–45. https://doi.org/10.1016/j.foreco.2017.12.049.
Panagiotidis, D., Abdollahnejad, A., Surový, P., Chiteculo, V., 2017. Determining tree height and crown diameter from high-resolution UAV imagery. Int. J. Rem. Sens. 38 (8–10), 2392–2410. https://doi.org/10.1080/01431161.2016.1264028.
Piermattei, L., Karel, W., Wang, D., Wieser, M., Mokroš, M., Surový, P., Koreň, M., Tomaštík, J., Pfeifer, N., Hollaus, M., 2019. Terrestrial structure from motion photogrammetry for deriving forest inventory data. Rem. Sens. 11, 950. https://doi.org/10.3390/rs11080950.
Plowright, A., 2020. Canopy analysis in R using forest tools. https://cran.r-project.org/web/packages/ForestTools/vignettes/treetopAnalysis.html. (Accessed 9 March 2021).
Plowright, A., Roussel, J.R., 2020. Package 'ForestTools'. https://cran.r-project.org/web/packages/ForestTools/ForestTools.pdf. (Accessed 9 March 2021).
Puliti, S., Ene, L., Gobakken, T., Naesset, E., 2017. Use of partial-coverage UAV data in sampling for large scale forest inventories. Rem. Sens. Environ. 194, 115–126. https://doi.org/10.1016/j.rse.2017.03.019.
Puliti, S., Saarela, S., Gobakken, T., Ståhl, G., Næsset, E., 2018. Combining UAV and Sentinel-2 auxiliary data for forest growing stock volume estimation through hierarchical model-based inference. Rem. Sens. Environ. 204, 485–497. https://doi.org/10.1016/j.rse.2017.10.007.
Ramalho de Oliveira, L.F., Lassiter, H.A., Wilkinson, B., Whitley, T., Ifju, P., Logan, S.R., Peter, G.F., Vogel, J.G., Martin, T.A., 2021. Moving to automated tree inventory: comparison of UAS-derived lidar and photogrammetric data with manual ground estimates. Rem. Sens. 13, 72. https://doi.org/10.3390/rs13010072.
SAUEZM, 2021. SAUEZM presents the activity report for 2020. http://dazv.gov.ua/novini-ta-media/vsi-novyny/u-dazv-prozvituvali-pro-rezultati-roboti-za-2020-rik.html. (Accessed 9 March 2021).
Schepaschenko, D., Shvidenko, A., Shalaev, V., 2008. Biological Productivity and Carbon Budget of Larch Forests of Northern-East Russia. Moscow State Forest University, Moscow (in Russian). https://bit.ly/3baFlE9.
Shapiro, S.S., Wilk, M.B., 1965. An analysis of variance test for normality (complete samples). Biometrika 52, 591–611. https://doi.org/10.1093/biomet/52.3-4.591.
Shcheglov, A., Tsvetnova, O., Klyashtorin, A., 2014. Biogeochemical cycles of Chernobyl-born radionuclides in the contaminated forest ecosystems. Long-term dynamics of the migration processes. J. Geochem. Explor. 144, 260–266. https://doi.org/10.1016/j.gexplo.2014.05.026.
Su, H., Shen, W., Wang, J., Ali, A., Li, M., 2020. Machine learning and geostatistical approaches for estimating aboveground biomass in Chinese subtropical forests. For. Ecosyst. 7 (1), 64. https://doi.org/10.1186/s40663-020-00276-7.
Surový, P., Kuželka, K., 2019. Acquisition of forest attributes for decision support at the forest Enterprise level using remote-sensing techniques - a review. Forests 10, 273. https://doi.org/10.3390/f10030273.
Talerko, M., Kovalets, I., Lev, T., Igarashi, Y., Romanenko, O., 2021. Simulation study of radionuclide atmospheric transport after wildland fires in the Chernobyl Exclusion Zone in April 2020. Atmos. Pollut. Res. 12 (3), 193–204. https://doi.org/10.1016/j.apr.2021.01.010.
Trouvé, R., Bontemps, J.-D., Seynave, I., Collet, C., Lebourgeois, F., 2015. Stand density, tree social status and water stress influence allocation in height and diameter growth of *Quercus petraea* (Liebl.). Tree Physiol. 35 (10), 1035–1046. https://doi.org/10.1093/treephys/tpv067.
UNSCEAR, 2008. Sources and Effects of Ionizing Radiation. annex D., New York: United Nations. https://www.unscear.org/docs/reports/2008/11-80076_Report_2008_Annex_D.pdf.
van Laar, A., Akça, A., 2007. Forest Mensuration. Springer, Dordrecht. https://doi.org/10.1007/978-1-4020-5991-9.
Wallace, L., Lucieer, A., Malenovský, Z., Turner, D., Vopenka, P., 2016. Assessment of forest structure using two UAV techniques: a comparison of airborne laser scanning and structure from motion (SfM) point clouds. Forests 7, 62. https://doi.org/10.3390/f7030062.
Wang, X.-H., Zhang, Y.-Z., Xu, M.-M., 2019. A multi-threshold segmentation for tree-level parameter extraction in a deciduous forest using small-footprint airborne LiDAR data. Rem. Sens. 11, 2109. https://doi.org/10.3390/rs11182109.
White, J.C., Wulder, M.A., Vastaranta, M., Coops, N.C., Pitt, D., Woods, M., 2013. The utility of image-based point clouds for forest inventory: a comparison with airborne laser scanning. Forests 4, 518–536. https://doi.org/10.3390/f4030518.
Xu, Z., Li, W., Li, Y., Shen, X., Ruan, H., 2019. Estimation of secondary forest parameters by integrating image and point cloud-based metrics acquired from unmanned aerial

vehicle. J. Appl. Remote Sens. 14 (2), 022204 https://doi.org/10.1117/1.JRS.14.022204.

Yan, W., Guan, H., Cao, L., Yu, Y., Li, Ch, Lu, Jian Y., 2020. A self-adaptive mean shift tree-segmentation method Using UAV LiDAR data. Rem. Sens. 12 (3), 515. https://doi.org/10.3390/rs12030515.

Yoschenko, V.I., Kashparov, V.A., Protsak, V.P., Lundin, S.M., Levchuk, S.E., Kadygrib, A. M., Zvarich, S.I., Khomutinin, YuV., Maloshtan, I.M., Lanshin, V.P., Kovtun, M.V., Tschiersch, J., 2006. Resuspension and redistribution of radionuclides during grassland and forest fires in the Chernobyl exclusion zone: part I. Fire experiments. J. Environ. Radioact. 86, 143–163. https://doi.org/10.1016/j.jenvrad.2005.08.003.

Yoschenko, V., Kashparov, V., Melnychuk, M., Levchuk, S., Bondar, Y., Lazarev, M., Yoschenko, M., Farfán, E., Jannik, T., 2011. Chronic irradiation of Scots pine trees, pinus sylvestris) in the Chernobyl exclusion zone: dosimetry and radiobiological effects. Health Phys. 101 (4), 393–408. https://doi.org/10.1097/hp.0b013e3182118094.

Yoschenko, V., Kashparov, V., Ohkubo, T., 2019. Radioactive contamination in forest by the accident of Fukushima daiichi nuclear power plant: comparison with Chernobyl. In: Takenaka, C., Hijii, N., Kaneko, N., Ohkubo, T. (Eds.), Radiocesium Dynamics in a Japanese Forest Ecosystem. Springer, Singapore, pp. 3–22. https://doi.org/10.1007/978-981-13-8606-0_1.

Yoschenko, V., Kashparov, V., Ohkubo, T., 2020. Behavior of the chernobyl-derived radionuclides in forest ecosystems and effects of radiation. In: Konoplev, A., Kato, K., Kalmykov, S. (Eds.), Behavior of Radionuclides in the Environment II. Springer, Singapore, pp. 283–320. https://doi.org/10.1007/978-981-15-3568-0_6.

Zahawi, R.A., Dandois, J.P., Holl, K.D., Nadwodny, D., Reid, J.L., Ellis, E.C., 2015. Using lightweight unmanned aerial vehicles to monitor tropical forest recovery. Biol. Conserv. 186, 287–295. https://doi.org/10.1016/j.biocon.2015.03.031.

Zhao, P., Gao, L., Gao, T., 2020. Extracting forest parameters based on stand automatic segmentation algorithm. Sci. Rep. 10, 1571. https://doi.org/10.1038/s41598-020-58494-6.